Koopman-Based Event-Triggered Control from Data

Preprint, authors version

Zeyad M. Manaa[1,2], **Ayman M. Abdallah**[1,2], **Mohamed Ismail**[1,2], **and Samil El Ferik**[3,4]

[1]Department of Aerospace Engineering, King Fahd University of Petroleum and Minerals (KFUPM), Dhahran, Saudi Arabia
[2]Interdisciplinary Research Center for Aviation and Space Exploration, KFUPM
[3]Department of Control and Instrumentation Engineering, KFUPM
[4]Interdisciplinary Research Center for Smart Mobility and Logistics, KFUPM

Abstract

Event-triggered Control (ETC) presents a promising paradigm for efficient resource usage in networked and embedded control systems by reducing communication instances compared to traditional time-triggered strategies. This paper introduces a novel approach to ETC for discrete-time nonlinear systems using a data-driven framework. By leveraging Koopman operator theory, the nonlinear system dynamics are globally linearized (approximately in practical settings) in a higher-dimensional space. We design a state-feedback controller and an event-triggering policy directly from data, ensuring exponential stability in Lyapunov sense. The proposed method is validated through extensive simulation experiments, demonstrating significant resource savings.

Keywords Event-triggered control, data-driven control, Koopman operator, discrete-time, Lyapunov stability

1 Introduction

ETC is an implementation strategy in which the plant and its controller only exchange data when certain output- or state-related conditions are met. Event-triggered control seeks to reduce communication instances by concentrating on the real needs of the system. This contrasts with traditional, conservative time-triggered strategies that depend on fixed communication intervals. In situations where efficient use of resources is essential, such as networked and embedded control systems, this paradigm has gained increasing attention. ETC strategies, which offer improved system performance and resource savings in a variety of setups and control problems, have been developed in the literature thanks to the early results by Åarzén in [1], Eker, Hagander, and Åarzén in [2] and the work of Tabuada [3], and Heemels et al. [4].

parametric state-space models are the foundation of traditional control engineering literature, where the plant to be controlled must be identified modeled or identified firstly. These models use system data and are often derived from first principles or architecturally constrained system identification techniques. But in cases when first-principles models are intricate or hard to derive, they can only be considered as approximate representations of real systems, which inevitably leads to modeling errors. These errors impede accurate control design. They propagate through the analysis and implementation phases, ultimately degrading overall system performance.

By excluding the demand for explicit system identification and instead of leveraging data gathered from open-loop simulations/experiments for any system control analysis and design, data-driven control techniques serve as a promising alternative. Several data-driven techniques for creating state feedback controllers and illustrating system dynamics have been shown in recent works, such as those by da Silva et al. [5], and De Persis and Tesi [6]. These techniques greatly streamline the control design process and do not require constantly exciting input data. There are also numerous applications of data-driven control in fields such as robotics [7], aerospace [8], and power systems [9]. Other methods, when the model is completely unknown, such as SINDy [10] can be utilized to firstly get a nonlinear representation of the dynamics of the system. For example, this approach is applied to model the dynamics of: i) quadrotors' [11], ii) disease [12], iii) optics communication systems [13], iv) chemical processes [14], v) and robotics applications [15].

Alternatively, when first-principles or system identification methods fail, the controller can be constructed directly using the input, state/output data that are accessible. This approach, referred to as direct data-driven control, [16, 17, 18] constructs controllers directly from data. Although the literature is full of data-driven techniques for control, only a limited number of techniques exist in the current literature [19, 20, 21] for data-driven event-based control, particularly for nonlinear systems. Hence, there is a strong demand for comprehensive data-driven event-based control methods tailored for general nonlinear systems, particularly applicable to discrete-time systems in our case. In many cases, it is appropriate and feasible to formulate the control and triggering conditions as data-dependent Linear Matrix Inequality (LMI). Given that most of the existing literature on ETC is well developed for Linear Time Invariant (LTI) systems, we aim to globally linearize nonlinear systems by increasing the dimensional space in which they reside.

This is not entirely a new idea. In the 1930s, Koopman and von Neumann [22, 23] introduced a trade-off between the nonlinear nature of dynamical systems and their infinite-dimensional representations, which appear linear in the lifted space. Another resurgence of attention in mid 2000s in the work of Mezić and Banaszuk [24, 25] has led to new applications and studies using the idea in many fields including, robotics, fluid dynamics, epidemiology, [26, 27, 28, 29, 30, 31, 32, 33, 34] and many other fields due to the intersection between data science and the easy-to-access computational domain.

We consequently propose Koopman Operator-Based Event-Triggered Control (KOETC), a technique inspired by

Koopman Operator (KO) to acquire (approximately) global linear systems but in a higher dimensional space. Afterwards, we design the controller and the triggering policy for ETC for discrete-time linear systems directly from controlled system data, all together ensuring performance metrics (i.e. Lyapunov exponential stability).

1.1 Contributions

By combining Koopman operator theory with event-triggered control (ETC), this paper makes a contribution by introducing a Koopman-based approach to ETC for discrete-time nonlinear systems. Through the approximate global linearization of nonlinear dynamics made possible by this integration, the following direct, data-driven designs are made possible:

i) An event-triggering policy minimizes resource consumption by updating control actions only when required, reducing communication instances; and

ii) A state-feedback controller, which effectively stabilizes the system by utilizing the Koopman-lifted linear dynamics.

In comparison to time-triggered approaches, the KOETC framework reduces communication events in simulations while achieving stability in the Lyapunov sense.

The rest of this paper is structured to methodically construct and validate the suggested KOETC framework after the motivation and goals have been established. The preliminary information and notations that are necessary to comprehend our methodology are outlined in Section 2. In Section 3, the KOETC framework's design is examined in detail, including the triggering policy and data-driven controller. We provide simulation results in Section 4, which show how effective the approach is. Section 5 provide additional discussions on practical guidelines for the proposed method. Finally, Section 6 concludes the paper and outlines potential directions for future research.

2 PRELIMINARIES

2.1 Notations and Basic Definitions

Let $\mathbb{Z}_{\geq 0} := \{0, 1, 2, \dots\}$ denote the set of nonnegative integers, and let $\mathbb{Z}_{>0} := \mathbb{Z}_{\geq 0} \setminus \{0\}$ denote the set of positive integers. We denote by $\mathbb{R}$ the set of real numbers and use a similar notation as for $\mathbb{Z}$. The ℓ_2 norm of a vector (a finite sequence) is denoted by $\|\cdot\|$. The symbols I and $\underline{0}$ denote the identity matrix and the zero matrix, respectively. Given a symmetric matrix A, the notation $A \succ 0$ indicates that A is positive definite, while $A \succeq 0$ means that A is positive semi-definite. Similarly, $A \prec 0$ indicates that A is negative definite and $A \preceq 0$ means that A is negative semi-definite. For any matrix A, $A^\top$ denotes the transpose of A. The symbol $\mathcal{N}(\mu, \sigma^2)$ represents a normal distribution with mean μ and variance σ^2. Also, the symbol $\mathcal{U}(a, b)$ represents a normal distribution from the interval $[a, b]$. The symbol λ_i denotes an eigenvalue of a matrix.

2.2 Problem Overview

Consider the discrete time dynamical system

$$x_{k+1} = f(x_k, u_k), \tag{1}$$

where the state is $x_k \in \mathbb{R}^n$ and $u_k \in \mathbb{R}^m$ is the control input, each at time instant $k \in \mathbb{Z}_{\geq 0}$ with $n, m \in \mathbb{Z}_{>0}$, and f is a transition map such that $f : \mathbb{R}^n \times \mathbb{R}^m \mapsto \mathbb{R}^n$, which is generally nonlinear, unknown, and assumed to be stabilizable.

We consider a scenario in which the system in (1) is connected to a controller via a networked medium. Especially, the state readings are provided to the controller through a digital channel, and the controller has direct access to the actuators. The goal is to design a data-driven event-triggered state-feedback controller with gain $K \in \mathbb{R}^{m \times n}$ to stabilize the plant in (1) while abiding by a triggering policy that defines the instances $\{k_i\}_{i \in \mathcal{Z}}$ at which a transmission happens, with $\mathcal{Z} \subseteq \mathbb{Z}_{\geq 0}$. At time instant $k = 0$, assume a transmission occurs, so that $k_0 = 0$. In our settings, the controller is updated only upon the violation of some well-defined triggering policy in contrast to the nominal Time-triggered Control (TTC). The sequence $\{k_i\}_{i \in \mathcal{Z}}$ leads to aperiodic updates of the controller. The controller then follows a zero-order hold implementation that takes the form of[1]

$$u_k = K x_{k_i}, \quad k \in [k_i, k_{i+1}). \tag{2}$$

The state error takes into account the provided controller's zero-order hold mechanism.

$$e_k = x_{k_i} - x_k, \tag{3}$$

which can be seen as the deviation between the current state and the last time event (i) is triggered. We consider an event is triggered whenever the following inequality is violated

$$\|e_k\| \leq \gamma \|x_k\|, \tag{4}$$

where $\gamma > 0$ is a threshold parameter for the triggering policy. The policy in (4) is evaluated at every time instant k, and the control is updated only when the policy is violated. Fig. 1 provides an overview of the ETC framework. Here the plant $\mathcal{P}$ represents (1), the controller C represents the control law (2), and the event-triggering policy corresponds to (4).

2.3 Persistence of Excitation

Consider a carried out experiment for the system in (1) and its states and input data are recorded in the following way

$$\mathcal{D} := \{x_k, u_k : k \in [0, (T-1)] \cap \mathbb{Z}_{\geq 0}\},$$

where T is the final time of the experiment. Assume that $\mathcal{D}$ the dataset exists. Then, we define

$$U_0 := \begin{bmatrix} u_0 & u_1 & \dots & u_{T-1} \end{bmatrix} \in \mathbb{R}^{m \times T}, \tag{5a}$$

$$X_0 := \begin{bmatrix} x_0 & x_1 & \dots & x_{T-1} \end{bmatrix} \in \mathbb{R}^{n \times T}, \tag{5b}$$

$$X_1 := \begin{bmatrix} x_1 & x_2 & \dots & x_T \end{bmatrix} \in \mathbb{R}^{n \times T}. \tag{5c}$$

Assumption 1. *Assume $T \geq n + m$, the matrix $\begin{bmatrix} X \\ U_0 \end{bmatrix}$ has full row rank.* □

[1] To be more precise, the control law should be $u_k = K\xi(x_{k_i}), \quad k \in [k_i, k_{i+1})$,, where $\xi(x_{k_i})$ is the lifted state. Since we are introducing the vanilla event-triggered mechanism, we use the original state of the system for completeness. In our problem formulation, we adhere to $u_k = K\xi(x_{k_i})$, unless otherwise stated. The concept of lifting will be discussed in subsection 3.1.

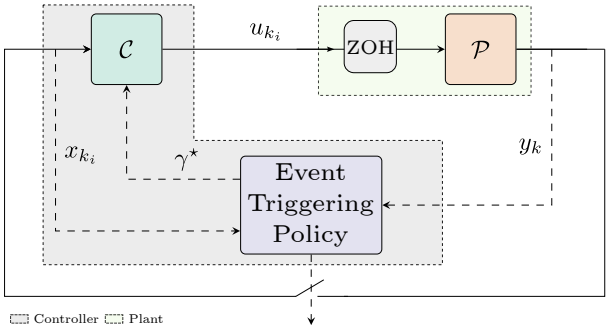

Figure 1: Block diagram visually providing representation that illustrates the core concept underlying ETC. It showcases various components and their interconnections, highlighting the essential principles and operational dynamics of the ETC framework.

Assumption 1 can be verified numerically for a given set $\mathcal{D}$. The results of Willems et al. [35] ensures, for discrete-time systems, the validity of assumption 1 as long as u is a persistently exciting signal.

3 FRAMEWORK

3.1 *Koopman operator theory*

Definition 1 (Koopman Operator (KO))**.** *Consider the system given in (1). The KO $\mathcal{K}_t$ is an infinite-dimensional operator*

$$\mathcal{K}_t\xi(x_k) = \xi \circ f(x_k), \tag{6}$$

which acts on $\xi \in \mathcal{H}$, where $\mathcal{H}$ is the space of observable functions $\xi : \mathbb{R}^n \to \mathbb{R}$ over the state space, where $\circ$ is the function composition. □

The KO acts on the Hilbert space $\mathcal{H}$ of all scalar measurement functions ξ and is, by definition, a *linear operator*, that is for any $\xi_1, \xi_2 \in \mathcal{H}$ and $\beta_1, \beta_2 \in \mathbb{R}$, we have

$$\begin{aligned}\mathcal{K}_t(\beta_1\xi_1, \beta_2\xi_2) &= \beta_1\xi_1 \circ f + \beta_2\xi_2 \circ f \\ &= \beta_1\mathcal{K}_t\xi_1 + \beta_2\mathcal{K}_t\xi_2,\end{aligned} \tag{7}$$

An infinite-dimensional space $\mathcal{H}$ of observable functions is used to represent a nonlinear system linearly using KO method [36]. This means that the dynamics are transformed from nonlinear and finite-dimensional to linear and infinite-dimensional when transitioning from the state-space model to the Koopman representation (see Fig. 2). However, we are interested in a finite-dimensional approximation of KO from a practical perspective. Several approximation methods are addressed in [37, 38].

To extend this analysis to controlled systems, there exist several methods including [39, 40]. In [39], the authors treated the controlled system as uncontrolled while treating the input as a system parameter. On the other hand, Korda and Mezić [40] dealt with the controlled system in an extended state-space to account for control.

Here, we briefly revisit the approach of [40]. In particular, consider the system in (1). Let $\ell(\mathfrak{U})$ be the space of all infinite vectors $u^\circ = \{u_k\}_{k=0}^\infty$ with the symbol $u_\circ \in \mathfrak{U}$ and $\mathfrak{U}$ being an input space. We denote the left shift operator by $\mathcal{G}^\star$ (e.g., $\mathcal{G}^\star u_k^\circ = u_{k+1}^\circ$). Also, define $\mathcal{X}$ to be an extended state such that, $\mathcal{X} = \begin{bmatrix} x_k & u_k^\circ \end{bmatrix}^\top$. So, the system in (1) can be reformulated as,

$$\mathcal{X}_{k+1} = \tilde{f}(\mathcal{X}) = \begin{bmatrix} f(x_k, u_0^\circ) \\ \mathcal{G}^\star u_k^\circ \end{bmatrix}. \tag{8}$$

If $\tilde{\xi} \in \mathcal{H} : \mathbb{R}^n \times \mathbb{R}^m \to \mathbb{R}$ be a new version of the predefined observable function, the Koopman operator $\mathcal{K}_t : \mathcal{H} \to \mathcal{H}$ for the controlled system turns out to be,

$$\mathcal{K}_t\tilde{\xi}(\mathcal{X}) = \tilde{\xi} \circ \tilde{f}(\mathcal{X}). \tag{9}$$

This was a demonstration of the extension from the uncontrolled systems to the controlled systems. From now on, we will use f, and ξ interchangeably between controlled and uncontrolled systems unless otherwise stated.

Also, KO provides (approximately, in a practical settings) global linear representation for nonlinear dynamics if the right set of observable functions is chosen in as shown in the following. Generally speaking, the observable functions are hard to identify. They can be found by many method including, but not limited to, brute-force trial and error in a specific basis for the Hilbert space (e.g., trying numerous polynomial functions or Fourier basis functions) or by prior knowledge about the system. Several efforts have been made on this matter [41, 42, 43, 44, 45, 46, 27] – among others. Our work relies heavily on the choice of the observable functions. Existing literature on how to choose such dictionary of function can be utilized in order to make best use of the presented paradigm. We discuss the effect of choosing the bad lifting dictionary in illustrative example 2 in section 4.2

Motivated by the preceding analysis, we employ the idea of lifting the nonlinear dynamics from its state-space to look linear in a higher-dimensional state-space.

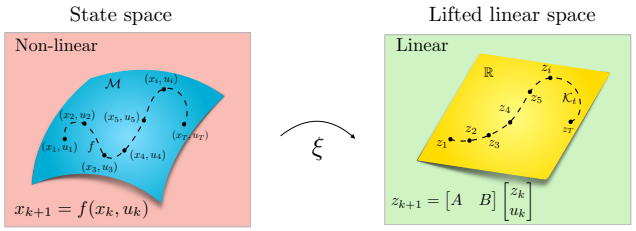

Figure 2: Illustration of the Koopman Operator: The red panel represents the generic nonlinear state-space. Conversely, the green panel represents the linear space.

Remark 1. *Since our method rely on the good choice of the observable functions, a blurry prior physical knowledge of the underlying plant, not necessarily a complete knowledge, but at least a knowledge that can describe the domain shape in which the system operates to design the observable functions could be of great benefit.* □

Remark 2. *At this stage of the work, we design the controller directly from the data. This step requires a set of observable functions that are satisfactory to approximate KO as discussed in remark 1. In the sense that we do not focus on the identification of the KO itself, we did not include discussion on such a topic. However, in more general scenarios, one may need*

to identify the operator for any purpose. Readers can refer to [47, 48]. □

Now, the collected set $\mathcal{D}$ should be revised. Instead of having the system's states only, we must consider the additional observable functions taking the form of $\Xi(x) = \begin{bmatrix}\xi_1(x) & \xi_2(x) & \dots & \xi_p(x)\end{bmatrix}^\top$. The observable functions $\Xi \in \mathbb{R}^p (p > n)$. Note that we only lift the state not the control. So the set $\mathcal{D}$ becomes

$$U_0 := \begin{bmatrix}u_0 & u_1 & \dots & u_{T-1}\end{bmatrix} \in \mathbb{R}^{m\times T}, \tag{10a}$$

$$Z_0 := \Xi(X_0) \in \mathbb{R}^{p\times T}, \tag{10b}$$

$$Z_1 := \Xi(X_1) \in \mathbb{R}^{p\times T}. \tag{10c}$$

Remark 3. *In response to this change, a slight modification of assumption 1, replacing the previous condition $T \geq n + m$ with $T \geq p + m$.* □

In response to this, the condition in (4) becomes,

$$\|e_k^\xi\| \leq \gamma \|\xi(x_k)\|, \tag{11}$$

where $e_k^\xi := \xi(x_k) - \xi(x_{k_i})$. Hence, after choosing the set of observable functions, the system in (1) can be now formulated as

$$z_{k+1} = Az_k + Bu_k, \tag{12a}$$

$$x_k = Cz_k. \tag{12b}$$

3.2 Event-triggered Control for the Lifted Representation of the Non-linear Dynamics

Consider the system given in (12), the globally linear version of the system in (1), subject to the controller (2) that results in

$$z_{k+1} = Az_k + BKz_{k_i} \tag{13a}$$

$$= Az_k + BKz_k + BKz_{k_i} - BKz_k \tag{13b}$$

$$= (A + BK)z_k + BKe_k, \quad \forall k \in [k_i,\ k_{i+1}), \tag{13c}$$

which can be understood as a closed-loop representation of the system in (12) with the state error.

An alternative representation of the event-triggered closed loop system should be derived to account for the data-driven nature of this work. In ref. [49] the authors derived a data-driven representation of the closed loop system without considering the matrix BK. On the other hand, Digge and Pasumarthy [20] developed a closed loop representation that allows dealing with the event-triggered formulation. The representation in [5] is modified to account for the lifted linear representation of the nonlinear dynamics.

Lemma 1 (Data-driven representation [20, 6])**.** *The equivalent data-driven closed loop representation of the system (13) under satisfaction of assumption 1 and where*

$$\begin{bmatrix}I\\K\end{bmatrix} = \begin{bmatrix}Z_0\\U_0\end{bmatrix} L, \text{ and } \begin{bmatrix}0\\K\end{bmatrix} = \begin{bmatrix}Z_0\\U_0\end{bmatrix} N, \tag{14}$$

holds, takes the following form

$$z_{k+1} = Z_1 L z_k + Z_1 N e_k, \tag{15}$$

where L and N are $T \times p$ matrices. □

Proof. Let assumption 1 be satisfied. Hence, by the Rouché-Capelli theorem, there exist matrices L and N that satisfy (14). So, another representation of (15) can be written as

$$z_{k+1} = \begin{bmatrix}A & B\end{bmatrix}\begin{bmatrix}I\\K\end{bmatrix} z_k + \begin{bmatrix}A & B\end{bmatrix}\begin{bmatrix}0\\K\end{bmatrix} e_k.$$

Using (14), the closed-loop system is given by

$$z_{k+1} = \underbrace{\begin{bmatrix}A & B\end{bmatrix}\begin{bmatrix}Z_0\\U_0\end{bmatrix}}_{Z_1} L z_k + \underbrace{\begin{bmatrix}A & B\end{bmatrix}\begin{bmatrix}Z_0\\U_0\end{bmatrix}}_{Z_1} N e_k.$$

Therefore, the data-driven representation of the closed-loop system (13) obtained as stated in (14).

This formulation can be considered as a reparametrization of the system in (13) in terms of data. In other words, no need for the prior explicit system identification step. Having established this formulation, we now proceed to derive the condition for system (15) to be exponentially stable in Lyapunov sense. A linear system described by $z_{k+1} = Az_k$, where $A \in \mathbb{R}^p$, is considered exponentially stable if there exists a function $V : \mathbb{R}^p \to \mathbb{R}$ defined by $V(z_k) = z_k^\top S z_k$ with $S \succ 0$ and symmetric, such that $V(z_{k+1}) \leq \alpha V(z_k)$ along the system's trajectories for all $k \geq 0$ and for some $\alpha \in \mathcal{A} := (0, 1] \subset \mathbb{R}$.

Remark 4. *For unstable systems, the choice of α is critical as it impacts the values of the controller gain $K(\alpha)$ which must satisfy the necessary conditions and thresholds to stabilize the system. This condition can be formalized as,*

$$\alpha^\star = \inf_{\alpha\in\mathcal{A}} \{\alpha : K(\alpha) \implies |\lambda_i| < 1,\ \forall \lambda_i\},$$

where the $K(\alpha)$ is the gains corresponding to one value of α on $\mathcal{A}$. □

Consider the classical Lyapunov candidate function described below, the exponential Lyaponuv stability criteria[2] is given by

$$\begin{bmatrix}z_k\\e_k\end{bmatrix}^\top \begin{bmatrix}L^\top Z_1^\top S Z_1 L - \alpha S & L^\top Z_1^\top S Z_1 N\\ N^\top Z_1^\top S Z_1 L & N^\top Z_1^\top S Z_1 N\end{bmatrix}\begin{bmatrix}z_k\\e_k\end{bmatrix} \leq 0 \tag{16}$$

In this work, the design of the ETC strategy should not violate the Lyapunov stability condition in (16) to ensure exponential stability.

3.3 Learning Controller From Data

Firstly, we design the controller gains to stabilize the globally linearized system. We consider the data-driven closed loop representation in (15) neglecting the error at this stage

$$z_{k+1} = Z_1 L z_k, \tag{17}$$

the controller gains can be designed directly from data, as discussed in [6, Section IV. A]. Further, the following theorem ensures the Lyaponuv stability condition.

Theorem 1 (Direct Controller Design)**.** *Let condition 1 hold. And by exploiting the results of lemma 1. Then any matrix G_1*

[2] The full analysis is given in the appendix.

that satisfy the following LMI,

$$\begin{bmatrix} Z_0G_1 & G_1^\top Z_1^\top \\ Z_1G_1 & Z_0G_1 \end{bmatrix} \geq 0 \tag{18}$$

results in

$$K = U_0G_1(Z_0G_1)^{-1} \tag{19}$$

which stabilizes the system (12). □

Proof. To check the stability in exponential decay of the system (17) with a rate α, implies

$$L^\top Z_1 S Z_1 L - \alpha S \preceq 0, \tag{20}$$

with L satisfying (14). Let $G_1 := LS^{-1}$, and pre- and post-multiply (20) by S^{-1}, the stability of the system can be guaranteed if there exists two matrices G_1 and S such that

$$\begin{aligned} &G_1^\top Z_1^\top S Z_1 G_1 - \alpha S^{-1} \preceq 0 \\ &KS^{-1} = U_0G_1 \\ &S^{-1} = Z_0G_1 \end{aligned}$$

Moreover, we use $S^{-1} = Z_0G_1$ and obtain

$$\begin{aligned} &G_1^\top Z_1^\top (Z_0G_1) Z_1G_1 - \alpha Z_0G_1 \preceq 0 \\ &Z_0G_1 \succ 0 \\ &K = U_0G_1(Z_0G_1)^{-1} \end{aligned}$$

Using Schur's complement lemma on the first inequality, we reach to (18) which results in gains given from (19) that exponentially stabilize the system.

3.4 Learning the Triggering Policy from Data

In the interval $[k_i,\ k_{i+1})$, it is essential that inequality (16), which ensures exponential convergence, is also satisfied. The following theorem derives a window for the parameter γ that ensures the stability of system (15).

Theorem 2 (Optimal Threshold)**.** *Assume that the condition 1 is satisfied. So, the relative threshold parameter γ for the event-triggered implementation (4) with the controller (19) can be calculated by solving for γ such that*

$$\begin{aligned} &\max_{q,G_2} \quad \gamma \\ &\textit{s.t.} \\ &\begin{bmatrix} \alpha Z_0G_1 & \underline{0} & G_1^\top Z_1^\top & \gamma Z_0G_1 \\ \underline{0} & qI & G_2^\top Z_1^\top & \underline{0} \\ Z_1G_1 & Z_1G_2 & Z_0G_1 & \underline{0} \\ \gamma Z_0G_1 & \underline{0} & \underline{0} & qI \end{bmatrix} \succeq \underline{0}, \\ &q > 0, \quad Z_0G_2 = 0, \quad UG_2 - qK = 0, \end{aligned} \tag{21}$$

which will result in stability of the system (15) in exponential behaviour. □

Proof. For exponential stability during event-triggered control, whenever the triggering condition (4) is met, the condition (16), which guarantees stability, must hold as well. This relationship can be encoded using the S-procedure [50]. According to the S-procedure, (4) implies (16) if there exists a constant $\eta \geq 0$ such that:

$$\eta \begin{bmatrix} -\gamma^2 I & \underline{0} \\ \underline{0} & I \end{bmatrix} \preceq \begin{bmatrix} L^\top Z_1^\top S Z_1 L - \alpha S & L^\top Z_1^\top S Z_1 L \\ L^\top Z_1^\top S Z_1 L & L^\top Z_1^\top S Z_1 L \end{bmatrix}.$$

Using Schur's complement, and post- and pre-multiplying by the $\mathtt{diag}(S^{-1}, I, I)$, we derive:

$$\begin{bmatrix} -\eta\gamma^2 S^{-2} + \alpha S^{-1} & \underline{0} & S^{-1}L^\top Z_1^\top \\ \underline{0} & \eta I & N^\top Z_1^\top \\ Z_1 L S^{-1} & Z_1 N \eta^{-1} & S^{-1} \end{bmatrix} \succeq \underline{0}.$$

By changing the variables $G_1 = LS^{-1}$, $G_2 = \eta^{-1}N$, $q = \eta^{-1}$, and $S^{-1} = Z_0G_1$, we arrive at the LMI:

$$\begin{bmatrix} \alpha Z_0G_1 & \underline{0} & G_1^\top Z_1^\top & \gamma Z_0G_1 \\ \underline{0} & qI & G_2^\top Z_1^\top & \underline{0} \\ Z_1G_1 & Z_1G_2 & Z_0G_1 & \underline{0} \\ \gamma Z_0G_1 & \underline{0} & \underline{0} & qI \end{bmatrix} \succeq \underline{0}.$$

The result of theorem 2 allows to maximize γ over the variables G_2 and q. The result also implies that any $\gamma \in [0, \gamma^\star)$ stabilizes the system, where $\gamma^\star$ is the solution for (21).

Now, we have all the components put together. A detailed algorithm for the entire process is given in algorithm 1.

Algorithm 1 Koopman Operator-Based Event-Triggered Control

Require: α, X_0, X_1, and U_0
1: Lift X_0, and X_1 via (10 b, and c)
2: Solve for G_1 in the LMI given in (18)
3: Solve for the controller gain K in (19)
4: Maximize the threshold parameter γ to get $\gamma^\star$ in (21)
5: Choose any $\gamma \in [0, \gamma^\star]$, (typically the max. value gives wider inter-event time window)
6: **return** $\gamma^\star$, and K

4 ILLUSTRATIVE SIMULATIONS AND RESULTS

In this section, three numerical examples are selected to illuminate distinct aspects of the proposed algorithm. Example 1 in Sec. 4.1 admits exact linearisation through a suitably chosen observable, making it an effective test bed for parameter studies. In this setting, we investigate how the decay rate α influences performance by tracking the peak discrete derivative of the Lyapunov function, and we assess the algorithm's ability to stabilise the system from a range of initial conditions. Additionally, example 2 in Sec. 4.2 addresses a system for which, to the best of the authors' knowledge, no observable yields a closed-form exact linearisation. This case isolates the consequences of observable selection and highlights how the proposed method behaves when exact linearisation is unavailable. Finally, example 3 in Sec. 4.3 demonstrates the method's generality for linear systems, as formalised in the corresponding section.

Following this section, we provide additional notes regarding some critical aspects of the proposed method.

4.1 Illustrative Example 1: Proof of Concept

We consider a case of nonlinear system with slow manifold used in relative works [51, 52, 53]:

$$\begin{bmatrix} x_1 \\ x_2 \end{bmatrix} \mapsto \begin{bmatrix} \rho x_1 \\ \kappa x_2 + (\rho^2 - \kappa)x_1^2 + u \end{bmatrix}. \tag{22}$$

In this scenario, there exists a polynomial stable manifold defined as $x_2 = x_1^2$. Within the Koopman-inspired framework, if the correct observable functions were chosen such that $\Xi(x) = \begin{bmatrix} x_1 & x_2 & x_1^2 \end{bmatrix}^\top$, the nonlinear system in (22) can be expressed linearly as

$$\begin{bmatrix} z_1 \\ z_2 \\ z_3 \end{bmatrix}_{k+1} = \begin{bmatrix} \rho & 0 & 0 \\ 0 & \kappa & (\rho^2 - \kappa) \\ 0 & 0 & \rho^2 \end{bmatrix} \begin{bmatrix} z_1 \\ z_2 \\ z_3 \end{bmatrix}_k + \begin{bmatrix} 0 \\ 1 \\ 0 \end{bmatrix} u_k \tag{23}$$

Considering the parameters for the system, $\rho = 0.6$, and $\kappa = 1.2$, the corresponding eigenvalues are $\lambda_1 = 0.6$, $\lambda_2 = 1.2$, and $\lambda_3 = 0.36$. Since $\lambda_2 > 1$, the system exhibits instability and the goal is to stabilize the trajectory around the origin. We collected the data for $T = 45$ which is enough for assumption 1 to hold – on a theoretical note, $T \geq m + p$ samples should be enough (i.e. in this example $T \geq 4$) to obey assumption 1. Therefore, $T = 4$ should work. The input signal is drawn from a normal distribution following $u \sim \mathcal{N}(0, 1)$.

Then, after deploying the steps in algorithm 1, we obtain $K = \begin{bmatrix} 0.0206 & -1.1109 & -0.1530 \end{bmatrix}$, which in turn gives $\gamma^\star = 0.7664$. We simulated the system for both ETC, and TTC and illustrated the behavior in Fig. 3. All the results depicted in Fig. 3, are acquired after pulling the states back from the higher-dimensional space, in this case from $\mathbb{R}^3$ to $\mathbb{R}^2$, by applying (12b) with $C = \begin{bmatrix} I_2 & 0 \\ 0 & 0 \end{bmatrix}$.

Fig. 3(a), illustrates the state evolution x_1 and x_2 against time under both ETC and TTC techniques. The trajectories for ETC demonstrate excellent tracking performance in comparison with the nominal TTC. This highlights the efficacy of the developed event-triggered approach in maintaining system stability while minimizing unnecessary updates.

Also, in Fig. 3(b), the graph shows that $\|e_k\|$ remains consistently below $\gamma\|x_k\|$, satisfying the triggering condition. As shown in Fig. 3(c), the substantial reduction in communication instances (40%) addresses potential concerns regarding communication overhead in practical implementations.

Finally, as noted from the numerical results, ETC not only achieves comparable performance to TTC but does so with fewer communication instances (about 40 compared to 100) and lower control cost (approximately 0.203 vs. 0.210), which supports our hypotheses. Another note in our experiment, both Koopman based linearization ETC and TTC have control cost much lower than the traditional Taylor linearization technique, consistent with the results of Brunton et al. [51].

For this example, we want to thoroughly examine ammd understand the influence of various parameters on the system's behavior and stability. This includes analysis of how different initial conditions and the parameter α impact the system dynamics. We explore these effects through a series of extensive simulations, designed to provide a comprehensive view of the system's response under a range of scenarios to enrich our theoretical insights and understanding.

Initially, we assessed the robustness of the algorithm by simulating ten different random initial conditions drawn from a uniform distribution $\sim \mathcal{U}(-5, 5)$. Fig. 4 shows the behavior of both x_1 and x_2 while starting with those random initial conditions. The figures show that while the initial conditions varies significantly, the behaviour of the system states stabilizes in a finite amount of time. An interesting observation from the same figure is that the error decay rate between the state and the reference in the log scale is nearly linear, supporting the paper's earlier demonstration of the exponential error decaying property.

Subsequently, the initial conditions were fixed at $x_0 = \begin{bmatrix} 0.5 & -0.4 \end{bmatrix}$ simulations were conducted across a fine grid of different α values ranging from 0.4 to 1. The choice of 0.4 as the starting value is informed by empirical observations, which indicate that this value represents the minimum threshold necessary to achieve an adequate gain for system stabilization, as detailed in remark 4. Fig. 5 demonstrates that for each value of α, there is no violation in the rate of Lyapunov function decay. The values on the x-axis in this figure must not exceed their corresponding values on the y-axis (i.e. they cannot cross the line $\max\left(V(k+1)/V(k)\right) = \alpha$). In other words, no deviation from the expected decaying behavior is observed.

In terms of time analysis, using a persistently excited signal sequence of length 45, the controller learning process took 0.4 seconds on an M2 MacBook Air, demonstrating the algorithm's practical efficiency. Similarly, learning the triggering policy under the same setup was achieved in 0.49 seconds.

4.2 Illustrative Example 2: Polynomial System

In this example, we consider a discrete-time nonlinear polynomial system defined as:

$$\begin{bmatrix} x_1 \\ x_2 \end{bmatrix} \mapsto \begin{bmatrix} ax_1 + bx_1^2 + cx_2 \\ dx_1x_2 + ex_2^2 + u \end{bmatrix}, \tag{24}$$

with parameters $a = 1.05$, $b = 0.1$, $c = 0.5$, $d = 0.25$, and $e = 0.08$. For this system, data were collected for $T = 150$ which is sufficient for assumption 1 to hold. In this example, we gather the data in a closed-loop manner inspired by Ref. [54] practical guidelines. In their work, they gather the identification data using a controller architecture similar to the one intended for design. For example, in the current example, we wish to design a stabilizing controller in the form of $u = Kz$. Therefore, we adopt a closed loop controller of a similar structure, $u = \tilde{K}z$, where the over all signal is perturbed by a random signal to ensure excitation. Perturbed trajectories are generated starting from a nonzero initial condition. The choice of the observable functions are motivated by the nonlinear terms in the system plus higher order polynomials as follows: $\Xi(x) = \begin{bmatrix} 1 & x_1 & x_2 & x_1^2 & x_1x_2 & x_2^2 & x_1^3 & x_2^3 & x_1^3 & x_2^3 \end{bmatrix}^\top$. The addition of the higher polynomials in the dictionary of the observable functions helped to reduce the steady state error as shown in Fig. 7. With the previous parameters and the choosing observables, in addition to choosing $\alpha = 0.7$, we proceed to apply Algorithm 1. As a result, we got $K =$

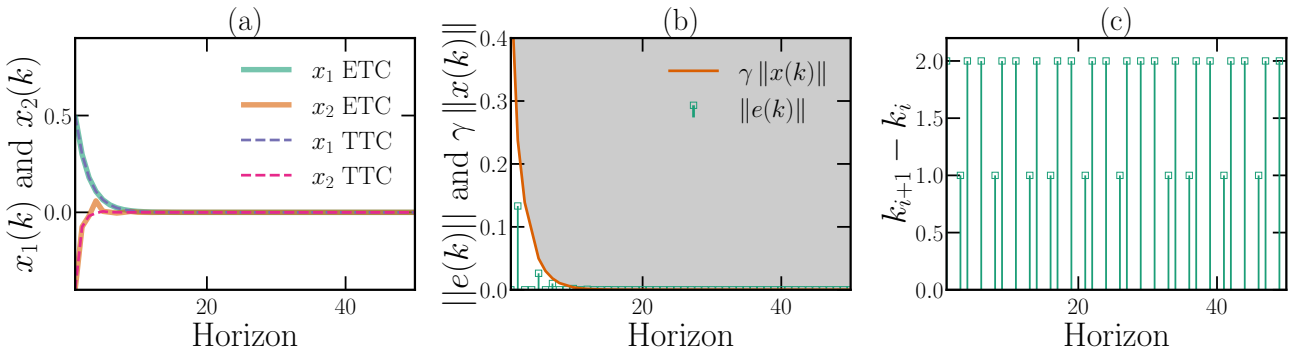

Figure 3: Results of the illustrative example 1. (a) Behaviour of state x_1 and x_2 for both ETC and TTC over the horizon. (b) Norms of the error $\|e_k\|$ and the threshold parameter $\gamma\|x_k\|$. (c) Inter-event times $k_{i+1} - k_i$ showing the intervals between successive events.

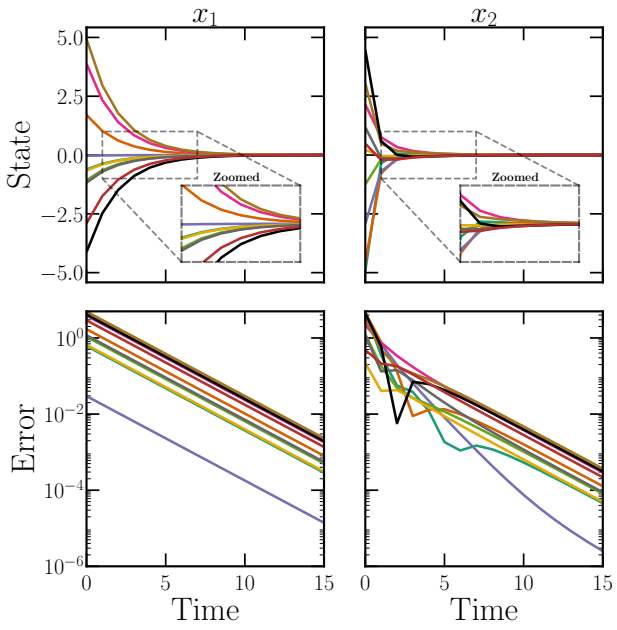

Figure 4: A simulation of ten random initial conditions drawn from a uniform distribution $X \sim \mathcal{U}(-5, 5)$. The figure shows the behaviour of x_1 (left), and x_2 (right).

$$\begin{bmatrix} -0.8742 & -0.3989 & -0.3779 & -0.5845 & -0.1581\ldots \\ \ldots 0.0301 & 0.0463 & -0.0157 & 0.0084 & -0.0071 \end{bmatrix},$$

and $\gamma = 0.2237$. The corresponding results and the behavior of the system are shown in Fig. 6. Although the interpretations of these results are quiet similar to that of subsection 4.1, we still need to asses the choice of the observable functions; since the system does not obey a choice of observables that exactly linearize the nonlinear system in a closed from as done in subsection 4.1. This is known as the closure problem.

To asses the effect of observable functions, we tested multiple cases under different observables. We adhere to monomial lifting functions with increasing order. Firstly, one can see the weak representation of a first-order polynomial for observable functions. This means that we implicitly assume that the nonlinear system in (24) can be well represented using linear observables, which is not evident from the most left bar of Fig. 7 following our understanding. Furthermore, a clear decreasing pattern appears for the steady state error as the degree number increases from 2 to 5. Surprisingly, the steady state error starts to increase at degree 6 which is a sign of overfitting. Consequently, increasing the number of observables does not guarantee a good representation. Further discussion on this will be provided in subsection 5.1.

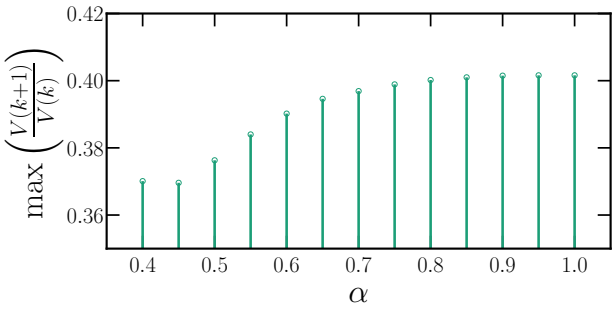

Figure 5: The relationship between α and the Lyapunov function decay rate. Simulations confirm no violations in the decay rate, as all points lie below the boundary $\max\left(V(k+1)/V(k)\right) = \alpha$, ensuring system stability across the tested α range.

4.3 *Illustrative Example 3: Linear Case Note*

In this example, we consider the discrete-time linear system (originally presented in [20])

$$x_{k+1} = Ax_k + Bu_k,$$

with $x_k \in \mathbb{R}^2$ and u_k generated from a random control signal within the interval $[-3, 3]$. The system matrices are given by $A = \begin{bmatrix} 0.91 & 0.0995 \\ 0.02 & 0.99 \end{bmatrix}$, $B = \begin{bmatrix} 0.01 \\ -0.184 \end{bmatrix}$, and the simulation is performed over 20 data points to learn a controller gain K with $\alpha = 0.9$ as well as the triggering threshold γ. Under the choice of the observable functions as identity, the gain K and an event-triggering threshold γ are computed according to the

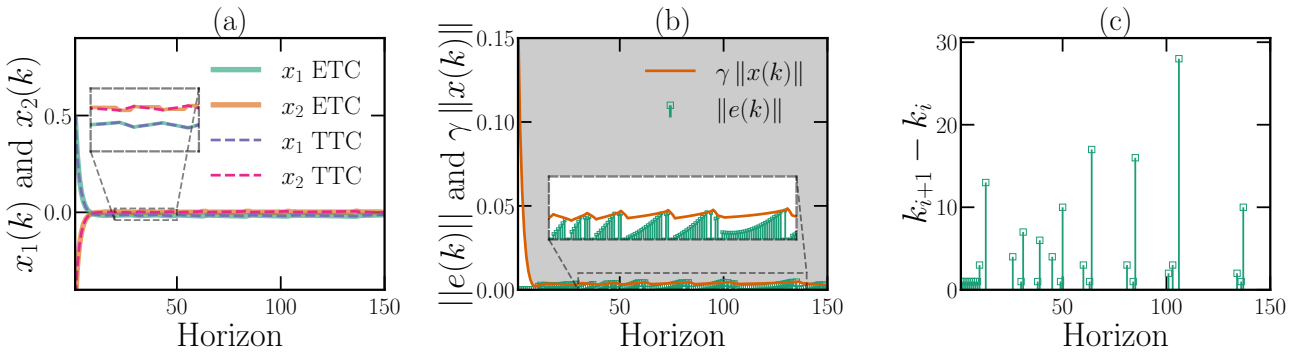

Figure 6: Results of the illustrative example 2. (a) Behaviour of state x_1 and x_2 for both ETC and TTC over the horizon. (b) Norms of the error $\|e_k\|$ and the threshold parameter $\gamma\|x_k\|$. (c) Inter-event times $k_{i+1} - k_i$ showing the intervals between successive events.

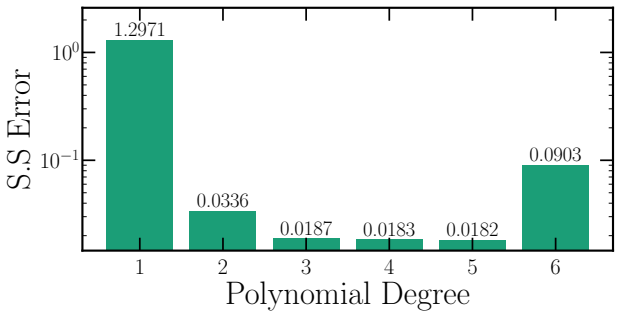

Figure 7: Steady-state error versus polynomial degree of the lifting function used for controller synthesis.

framework in 1 and resulted in $K = \begin{bmatrix}0.3820 & 0.8179\end{bmatrix}$ and $\gamma = 0.4653$.

Notably, if the observable functions are chosen as the identity, then the algorithm directly addresses the linear dynamics without any additional lifting. In this case, our approach reduces to the classical linear control and event-triggered control framework as presented in [20]. The results of this example are depicted in Fig. 8 which matches with excellent agreement the results in Digge and Pasumarthy [20] work.

5 Discussions

5.1 *On the choice of the observable functions*

We devote this section to discussing some notes towards practical discussion of the selection of observable functions. As mentioned earlier in the paper, the choice of the lifting functions is critical part in designing the direct data driven controller that abides to an additional event-triggering role. This is also noted in the literature covering the Koopman operator [55]. The authors noted that the rate of convergence of the Koopman based identification method depends on the dictionary of the observable functions which they refer to as trials or basis functions. In their work they assume the basis functions spans the subspace of the observables. One can motivate the choice of the observables in our methods using similar approach. Possible choices of the observables are: polynomials, and Radial Basis Functions (RBFs). As advised by the authors, polynomials are a good option to be used for the system defined on $\mathbb{R}^N$, and the RBFs are a good candidate for systems defined on irregular domains.

Recently, considerable research effort has been devoted to the idea of finding a good set of observables. Namely:

i) employing deep learning autoencoders [43, 56],

ii) local higher-order derivatives of the nonlinear system [46] (though it requires a symbolic expression of the nonlinear system),

iii) motivating the choice of observables by analytical constructions in [44] and [57]. In [57] the method is specifically tailored to certain robotic systems by exploiting the topological spaces of these systems to guide the construction of Hermite polynomial-based observables,

iv) avoiding explicit basis selection by defining observables implicitly in a reproducing kernel Hilbert space [58, 59] using kernel functions (e.g. Gaussian kernel $k(x, y) = e^{\|x-y\|^2/2\sigma^2}$).

Building on the above discussion, how to choose an appropriate set of observables remains an important, yet open, question. Nonetheless, many of the methods discussed above have shown practical effectiveness.

5.2 *On the Controller Synthesis*

In this section we refer back to the examples in subsection 4.1, and Equation 4.2. Although the feedback control law looks linear on the observable space z, it could be looked to it as a nonlinear controller on the original state x. For example, the illustrative example 1 in subsection 4.1, the designed controller in terms of the original states can be interpreted as,

$$\begin{aligned} u &= \begin{bmatrix}K_1 & K_2\end{bmatrix}\begin{bmatrix}x_1\\ x_2\end{bmatrix} + K_3 x_1^2 \\ &= 0.0206\ x_1 - 1.1109\ x_2 - 0.1540\ x_1^2 \end{aligned} \tag{25}$$

where the third term indicates the nonlinearity imposed by the choice of the nonlinear observable function x_2^2. Similar analysis could be done for example 2 by examining the effect of the

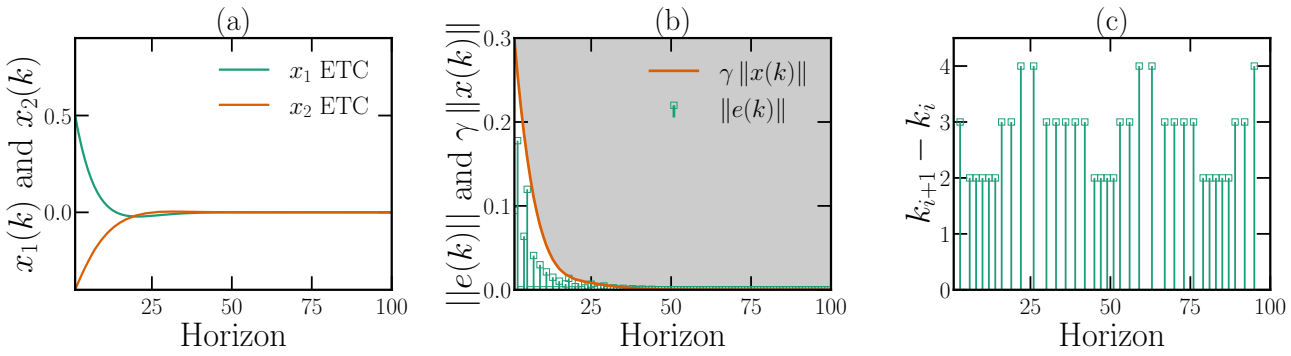

Figure 8: Results of the illustrative example 3. (a) Behaviour of state x_1 and x_2. (b) Norms of the error $\|e_k\|$ and the threshold parameter $\gamma\|x_k\|$. (c) Inter-event times $k_{i+1} - k_i$ showing the intervals between successive events.

observables on the control law. On the other hand, in example 3 in subsection 4.3, the control law remains linear as it originally introduced.

We recommend that the future research should look into how to optimally design the controller gain and also a policy that respects the system stability.

6 Conclusion

To sum up, this study proposes an event-triggered control approach based on data-driven methods for discrete-time nonlinear systems. By lifting the nonlinear dynamics into a higher-dimensional linear representation inspired by the KO theory, the method makes it possible to create an event-triggered controller driven by data. Through the development of a closed-loop system and the implementation of a triggering strategy, the proposed method stabilizes the plant with less frequent control updates.

The event-triggered closed-loop system's exponential stability is guaranteed by the stability analysis, which is based on the Lyapunov criterion. Numerical simulations and theoretical analysis are used to show how effective the suggested strategy is. This work creates opportunities for real-world applications in networked control systems and advances event-triggered control techniques for nonlinear systems.

The foundations provided by this work shall allow dealing with many other scenarios including, when the plant (discrete or continuous) include time varying parameters, when the full state measurements are not available, or when policies other than the zero-order hold is used. Additionally, examining the various lifting techniques available in the literature is important, as well as, testing the scalability of the solution.

A Lyapunov Stability Analysis

This subsection of the appendix presents the exponential stability of the system given by

$$z_{k+1} = Z_1 L z_k + Z_1 N e_k \tag{26}$$

in a Lyapunov sense with the candidate $V(k) = z_k^\top S z_k$.

First, $V(z_{k+1})$ can be computed as follows

$$\begin{aligned} V(z_{k+1}) &= (Z_1 L z_k + Z_1 N e_k)^\top S\, (Z_1 L z_k + Z_1 N e_k) \\ &= z_k^\top L^\top Z_1^\top S Z_1 L z_k + z_k^\top L^\top Z_1^\top S Z_1 N e_k + \dots \\ &\dots e_k^\top N^\top Z_1^\top S Z_1 L z_k + e_k^\top N^\top Z_1^\top S Z_1 N e_k \end{aligned} \tag{27}$$

Lyapunov exponential stability condition with convergence rate α can be reached by defining $V(z_{k+1}) \leq \alpha V(z_k)$. This leads to the following identity based on the candidate Lyapunov function

$$\begin{aligned} &z_k^\top L^\top Z_1^\top S Z_1 L z_k + z_k^\top L^\top Z_1^\top S Z_1 N e_k + \dots \\ &\dots e_k^\top N^\top Z_1^\top S Z_1 L z_k + e_k^\top N^\top Z_1^\top S Z_1 N e_k \leq \alpha z_k^\top S z_k \end{aligned} \tag{28}$$

By defining $v = \left[\begin{smallmatrix} z_k \\ e_k \end{smallmatrix}\right]$, Eqn. (28) can be written in the form of $v^\top \Psi v \leq 0$, where

$$\Psi = \begin{bmatrix} L^\top Z_1^\top S Z_1 L - \alpha S & L^\top Z_1^\top S Z_1 N \\ N^\top Z_1^\top S Z_1 L & N^\top Z_1^\top S Z_1 N \end{bmatrix} \tag{29}$$

Therefore, the Lyapunov stability condition for the system can be written as

$$\begin{bmatrix} z_k \\ e_k \end{bmatrix}^\top \begin{bmatrix} L^\top Z_1^\top S Z_1 L - \alpha S & L^\top Z_1^\top S Z_1 N \\ N^\top Z_1^\top S Z_1 L & N^\top Z_1^\top S Z_1 N \end{bmatrix} \begin{bmatrix} z_k \\ e_k \end{bmatrix} \leq 0 \tag{30}$$

If condition (30) is satisfied, it then guarantees exponential stability of the system with convergence rate α.

References

[1] Karl-Erik Åarzén. A simple event-based PID controller. *IFAC Proceedings Volumes*, 32(2):8687–8692, 1999.

[2] Johan Eker, Per Hagander, and Karl-Erik Årzén. A feedback scheduler for real-time controller tasks. *Control Engineering Practice*, 8(12):1369–1378, 2000.

[3] Paulo Tabuada. Event-triggered real-time scheduling of stabilizing control tasks. *IEEE Transactions on Automatic control*, 52(9):1680–1685, 2007.

[4] Wilhelmus PMH Heemels, Karl Henrik Johansson, and Paulo Tabuada. An introduction to event-triggered and self-triggered control. In *2012 ieee 51st ieee conference*

on decision and control (cdc), pages 3270–3285. IEEE, 2012.

[5] Gustavo R Gonçalves da Silva, Alexandre S Bazanella, Charles Lorenzini, and Luciola Campestrini. Data-driven LQR control design. *IEEE control systems letters*, 3(1): 180–185, 2018.

[6] Claudio De Persis and Pietro Tesi. Formulas for data-driven control: Stabilization, optimality, and robustness. *IEEE Transactions on Automatic Control*, 65(3):909–924, 2019.

[7] Lu Shi and Konstantinos Karydis. Enhancement for robustness of koopman operator-based data-driven mobile robotic systems. In *2021 IEEE International Conference on Robotics and Automation (ICRA)*, pages 2503–2510. IEEE, 2021.

[8] Carl Folkestad, Skylar X Wei, and Joel W Burdick. Quadrotor trajectory tracking with learned dynamics: Joint koopman-based learning of system models and function dictionaries. *arXiv preprint arXiv:2110.10341*, 2021.

[9] Yoshihiko Susuki, Igor Mezic, Fredrik Raak, and Takashi Hikihara. Applied koopman operator theory for power systems technology. *Nonlinear Theory and Its Applications, IEICE*, 7(4):430–459, 2016.

[10] Steven L Brunton, Joshua L Proctor, and J Nathan Kutz. Discovering governing equations from data by sparse identification of nonlinear dynamical systems. *Proceedings of the national academy of sciences*, 113(15):3932–3937, 2016.

[11] Zeyad M Manaa, Mohammed R Elbalshy, and Ayman M Abdallah. Data-driven discovery of the quadrotor equations of motion via sparse identification of nonlinear dynamics. In *AIAA SCITECH 2024 Forum*, page 1308, 2024.

[12] Yu Xin Jiang, Xiong Xiong, Shuo Zhang, Jia Xiang Wang, Jia Chun Li, and Lin Du. Modeling and prediction of the transmission dynamics of COVID-19 based on the SINDy-LM method. *Nonlinear Dynamics*, 105:2775–2794, 2021. ISSN 1573269X. Number: 3.

[13] Mariia Sorokina, Stylianos Sygletos, and Sergei Turitsyn. Sparse Identification for Nonlinear Optical Communication Systems: SINO Method. *Opt. Express*, 24(26):30433, December 2016. ISSN 1094-4087. doi: 10.1364/OE.24.030433. URL http://arxiv.org/abs/1701.01650. arXiv:1701.01650 [physics].

[14] Bhavana Bhadriraju, Mohammed Saad Faizan Bangi, Abhinav Narasingam, and Joseph Sang Il Kwon. Operable adaptive sparse identification of systems: Application to chemical processes. *AIChE Journal*, 66(11), 2020. ISSN 15475905. doi: 10.1002/aic.16980. Number: 11.

[15] Dipankar Bhattacharya, Leo K. Cheng, and Weiliang Xu. Sparse Machine Learning Discovery of Dynamic Differential Equation of an Esophageal Swallowing Robot. *IEEE Transactions on Industrial Electronics*, 67(6):4711–4720, 2020. ISSN 15579948. doi: 10.1109/TIE.2019.2928239. Number: 6.

[16] Mario Sznaier. Control oriented learning in the era of big data. *IEEE Control Systems Letters*, 5(6):1855–1867, 2020.

[17] Marco C Campi, Andrea Lecchini, and Sergio M Savaresi. Virtual reference feedback tuning: a direct method for the design of feedback controllers. *Automatica*, 38(8): 1337–1346, 2002.

[18] Michel Fliess and Cédric Join. Model-free control. *International journal of control*, 86(12):2228–2252, 2013.

[19] Wenjie Liu, Jian Sun, Gang Wang, Francesco Bullo, and Jie Chen. Data-driven self-triggered control via trajectory prediction. *IEEE Transactions on Automatic Control*, 68 (11):6951–6958, 2023.

[20] Vijayanand Digge and Ramkrishna Pasumarthy. Data-driven event-triggered control for discrete-time LTI systems. In *2022 European Control Conference (ECC)*, pages 1355–1360. IEEE, 2022.

[21] Xin Wang, Julian Berberich, Jian Sun, Gang Wang, Frank Allgöwer, and Jie Chen. Model-based and data-driven control of event-and self-triggered discrete-time linear systems. *IEEE Transactions on Cybernetics*, 2023.

[22] Bernard O Koopman. Hamiltonian systems and transformation in hilbert space. *Proceedings of the National Academy of Sciences*, 17(5):315–318, 1931.

[23] Bernard O Koopman and J v Neumann. Dynamical systems of continuous spectra. *Proceedings of the National Academy of Sciences*, 18(3):255–263, 1932.

[24] Igor Mezić and Andrzej Banaszuk. Comparison of systems with complex behavior. *Physica D: Nonlinear Phenomena*, 197(1-2):101–133, 2004.

[25] Igor Mezić. Spectral properties of dynamical systems, model reduction and decompositions. *Nonlinear Dynamics*, 41:309–325, 2005.

[26] Daniel Bruder, Xun Fu, R Brent Gillespie, C David Remy, and Ram Vasudevan. Koopman-based control of a soft continuum manipulator under variable loading conditions. *IEEE robotics and automation letters*, 6(4):6852–6859, 2021.

[27] Giorgos Mamakoukas, Maria L Castano, Xiaobo Tan, and Todd D Murphey. Derivative-based koopman operators for real-time control of robotic systems. *IEEE Transactions on Robotics*, 37(6):2173–2192, 2021.

[28] Xuehong Zhu, Chengjun Ding, Lizhen Jia, and Yubo Feng. Koopman operator based model predictive control for trajectory tracking of an omnidirectional mobile manipulator. *Measurement and Control*, 55(9-10):1067–1077, 2022.

[29] Naoto Komeno, Brendan Michael, Katharina Küchler, Edgar Anarossi, and Takamitsu Matsubara. Deep koopman with control: Spectral analysis of soft robot dynamics. In *2022 61st Annual Conference of the Society of Instrument and Control Engineers (SICE)*, pages 333–340. IEEE, 2022.

[30] Minghao Han, Jacob Euler-Rolle, and Robert K Katzschmann. Desko: Stability-assured robust control

with a deep stochastic koopman operator. In *International Conference on Learning Representations*, 2021.

[31] Zeyad M Manaa, Ayman M Abdallah, Mohammad A Abido, and Syed S Azhar Ali. Koopman-LQR Controller for Quadrotor UAVs from Data. *arXiv preprint arXiv:2406.17973*, 2024.

[32] Ramij Raja Hossain, Rahmat Adesunkanmi, and Ratnesh Kumar. Data-driven linear koopman embedding for networked systems: Model-predictive grid control. *IEEE Systems Journal*, 2023.

[33] Thorben Markmann, Michiel Straat, and Barbara Hammer. Koopman-based surrogate modelling of turbulent rayleigh-b\'enard convection. *arXiv preprint arXiv:2405.06425*, 2024.

[34] Igor Mezić, Zlatko Drmač, Nelida Črnjarić, Senka Maćešić, Maria Fonoberova, Ryan Mohr, Allan M Avila, Iva Manojlović, and Aleksandr Andrejčuk. A koopman operator-based prediction algorithm and its application to covid-19 pandemic and influenza cases. *Scientific reports*, 14(1):5788, 2024.

[35] Jan C Willems, Paolo Rapisarda, Ivan Markovsky, and Bart LM De Moor. A note on persistency of excitation. *Systems & Control Letters*, 54(4):325–329, 2005.

[36] Marko Budišić, Ryan Mohr, and Igor Mezić. Applied koopmanism. *Chaos: An Interdisciplinary Journal of Nonlinear Science*, 22(4), 2012.

[37] Petar Bevanda, Stefan Sosnowski, and Sandra Hirche. Koopman operator dynamical models: Learning, analysis and control. *Annual Reviews in Control*, 52:197–212, 2021.

[38] Joshua L Proctor, Steven L Brunton, and J Nathan Kutz. Generalizing koopman theory to allow for inputs and control. *SIAM Journal on Applied Dynamical Systems*, 17(1):909–930, 2018.

[39] Sebastian Peitz, Samuel E Otto, and Clarence W Rowley. Data-driven model predictive control using interpolated koopman generators. *SIAM Journal on Applied Dynamical Systems*, 19(3):2162–2193, 2020.

[40] Milan Korda and Igor Mezić. Linear predictors for nonlinear dynamical systems: Koopman operator meets model predictive control. *Automatica*, 93:149–160, 2018.

[41] Samuel E Otto and Clarence W Rowley. Linearly recurrent autoencoder networks for learning dynamics. *SIAM Journal on Applied Dynamical Systems*, 18(1):558–593, 2019.

[42] Enoch Yeung, Soumya Kundu, and Nathan Hodas. Learning deep neural network representations for koopman operators of nonlinear dynamical systems. In *2019 American Control Conference (ACC)*, pages 4832–4839. IEEE, 2019.

[43] Bethany Lusch, J Nathan Kutz, and Steven L Brunton. Deep learning for universal linear embeddings of nonlinear dynamics. *Nature communications*, 9(1):4950, 2018.

[44] Marcos Netto, Yoshihiko Susuki, Venkat Krishnan, and Yingchen Zhang. On analytical construction of observable functions in extended dynamic mode decomposition for nonlinear estimation and prediction. In *2021 American Control Conference (ACC)*, pages 4190–4195. IEEE, 2021.

[45] Mason Kamb, Eurika Kaiser, Steven L Brunton, and J Nathan Kutz. Time-delay observables for koopman: Theory and applications. *SIAM Journal on Applied Dynamical Systems*, 19(2):886–917, 2020.

[46] Giorgos Mamakoukas, Maria Castano, Xiaobo Tan, and Todd Murphey. Local koopman operators for data-driven control of robotic systems. In *Robotics: science and systems*, 2019.

[47] Peter J Schmid. Dynamic mode decomposition of numerical and experimental data. *Journal of fluid mechanics*, 656:5–28, 2010.

[48] Joshua L Proctor, Steven L Brunton, and J Nathan Kutz. Dynamic mode decomposition with control. *SIAM Journal on Applied Dynamical Systems*, 15(1):142–161, 2016.

[49] Claudio De Persis, Romain Postoyan, and Pietro Tesi. Event-triggered control from data. *IEEE Transactions on Automatic Control*, 2023.

[50] Stephen P Boyd and Lieven Vandenberghe. *Convex optimization*. Cambridge university press, 2004.

[51] Steven L Brunton, Bingni W Brunton, Joshua L Proctor, and J Nathan Kutz. Koopman invariant subspaces and finite linear representations of nonlinear dynamical systems for control. *PloS one*, 11(2), 2016.

[52] Amit Surana and Andrzej Banaszuk. Linear observer synthesis for nonlinear systems using koopman operator framework. *IFAC-PapersOnLine*, 49(18):716–723, 2016.

[53] Amit Surana. Koopman operator based observer synthesis for control-affine nonlinear systems. In *2016 IEEE 55th Conference on Decision and Control*, pages 6492–6499. IEEE, 2016.

[54] Loi Do, Adam Uchytil, and Zdeněk Hurák. Practical guidelines for data-driven identification of lifted linear predictors for control. *arXiv preprint arXiv:2408.01116*, 2024.

[55] Matthew O Williams, Ioannis G Kevrekidis, and Clarence W Rowley. A data–driven approximation of the koopman operator: Extending dynamic mode decomposition. *Journal of Nonlinear Science*, 25:1307–1346, 2015.

[56] Jiacheng Ge, Yijun Xu, and Zaijun Wu. Deep learning-based construction of koopman observable functions for power system nonlinear dynamics. In *2024 IEEE Power & Energy Society General Meeting (PESGM)*, pages 1–5. IEEE, 2024.

[57] Lu Shi and Konstantinos Karydis. Acd-edmd: Analytical construction for dictionaries of lifting functions in koopman operator-based nonlinear robotic systems. *IEEE Robotics and Automation Letters*, 7(2):906–913, 2021.

[58] Matthew O Williams, Clarence W Rowley, and Ioannis G Kevrekidis. A kernel-based approach to data-driven koopman spectral analysis. *arXiv preprint arXiv:1411.2260*, 2014.

[59] Jonghyeon Lee, Boumediene Hamzi, Boya Hou, Houman Owhadi, Gabriele Santin, and Umesh Vaidya. Kernel methods for the approximation of the eigenfunctions of the koopman operator. *arXiv preprint arXiv:2412.16588*, 2024.